Atmospheric-pressure plasma jet texturing of C/C composites for improved joint strength

Mechanical Systems and Signal Processing

Predictive Dynamic Modeling and Analysis of Blisks Through Digital Representations Constructed Upon Precise Geometry Measurements

--Manuscript Draft--

Manuscript Number:	MSSP23-3511
Article Type:	Standard Research Article
Section/Category:	
Keywords:	blisks; geometric variances; finite element modeling; model reduction; forced response tests
Corresponding Author:	Biao Zhou Nanjing University of Aeronautics and Astronautics Nanjing, CHINA
First Author:	Biao Zhou
Order of Authors:	Biao Zhou
	Chengyu Xie
	Giuseppe Battiato
	Teresa Maria Berruti
Abstract:	Blade geometric variances generally have a significant impact on the structural dynamics of integrally bladed disks widely used in the advanced aero-engines. This paper presents a holistic research in regard to the predictive dynamic modelling, analysis and experimental verification for a blisk by taking advantage of the advanced 3D optical geometry measurement technology. Geometrically mistuned models (GMMs) are semi-automatically constructed upon the precisely measured blisk geometry by an efficient FE mesh updating strategy. They provide explicit, high-fidelity digital representations of the geometric variances within the integrally manufactured blisk. A `Sector Mode Assembling Reduction Technique' is developed and specifically tailored for efficient dynamic analysis of the large-sized GMMs at a relatively low computational cost and memory requirement. Intensive test campaigns, including forced response tests in the stationary/spinning rig under well-controlled laboratory conditions, are carried out for a full assessment of the GMMs' dynamic prediction capability. Experimental verification results show that the GMM is able to capture the modal dynamics and resonant vibration of the stationary/rotating blisk with satisfactory accuracy. The physical-reality-based GMM converted directly from the precise geometry measurement data can be considered as a viable and valuable tool for predictive vibration evaluation of blisks. However, its model accuracy exhibits a mode-related dependence on the mesh density. The tradeoff between model accuracy and prohibitive computational cost proved to be the bottleneck of this promising blisk modeling approach.
Suggested Reviewers:	Jie Yuan University of Southampton j.yuan@soton.ac.uk
	Bernd Beirow Brandenburg University of Technology Cottbus-Senftenberg beirow@b-tu.de
	Luigi Carassale University of Genoa luigi.carassale@unige.it
	Florence Nyssen Montreal Polytechnic florence.nyssen@polymtl.ca

Dear editorial board,

Please find enclosed the manuscript: "Predictive Dynamic Modeling and Analysis of Blisks Through Digital Representations Constructed Upon Precise Geometry Measurement", by Biao Zhou, Chengyu Xie, Giuseppe Battiato, Teresa Maria Berruti, to be submitted as an article for consideration of Mechanical Systems and Signal Processing.

It is well known that blade geometric variances generally have a significant impact on the structural dynamics of integrally bladed disks widely used in the advanced aero-engine. In this manuscript, we present a holistic research in regard to the predictive dynamic modelling, analysis and experimental verification for a blisk by taking advantage of the advanced 3D optical geometry measurement technology.

Specifically, Geometrically Mistuned Models (GMMs) are constructed upon the precisely measured blisk geometry by an efficient FE mesh updating strategy. They provide explicit, high-fidelity digital representations of the geometric variances within the integrally manufactured blisk. A ‘Sector Mode Assembling Reduction Technique’ is developed and specifically tailored for efficient dynamic analysis of the large-sized GMMs at a relatively low computational cost and memory requirement. Intensive test campaigns, including forced response tests in the stationary/spinning rig under well-controlled laboratory conditions, are carried out for a full assessment of the GMMs’ dynamic prediction capability.

We believe that this manuscript could be of interest to readers of Mechanical Systems and Signal Processing. In particular, this research gives the experimental evidence that the GMM converted directly from the precise geometry measurement data is able to capture the modal dynamics and resonant vibration of the stationary/rotating blisk with a very good level of accuracy.

The methods and correlation results presented in this paper are expected to push the frontier of the emerging geometric-mistuning modeling and dynamic analysis techniques for integrally bladed disks.

We hope that the editorial board will agree on the interest of this study.

Sincerely,

Biao Zhou on behalf of the authors.

Highlights

Predictive Dynamic Modeling and Analysis of Blisks Through Digital Representations Constructed Upon Precise Geometry Measurement

Biao Zhou, Chengyu Xie, Giuseppe Battiato, Teresa Maria Berruti

- Geometrically mistuned models (GMMs) are constructed upon measured blisk geometry.
- GMMs are dynamically reduced by a Sector Mode Assembling Reduction Technique.
- GMM's accuracy exhibits a mode-related dependence on the mesh density.
- GMMs are validated by forced response tests in the stationary/spinning rig.
- GMM captures resonant vibration of the stationary/rotating blisk with good accuracy.

Predictive Dynamic Modeling and Analysis of Blisks Through Digital Representations Constructed Upon Precise Geometry Measurements

Biao Zhou[a], Chengyu Xie[a], Giuseppe Battiato[b], Teresa Maria Berruti[b]

[a] *College of Energy and Power Engineering, Nanjing University of Aeronautics and Astronautics, 29 Yudao St., Nanjing, 210016, China*
[b] *Dipartimento di Ingegneria Meccanica e Aerospaziale, Politecnico di Torino, Corso Duca degli Abruzzi, 24, Torino, 10129, Italy*

Abstract

Blade geometric variances generally have a significant impact on the structural dynamics of integrally bladed disks widely used in the advanced aero-engines. This paper presents a holistic research in regard to the predictive dynamic modelling, analysis and experimental verification for a blisk by taking advantage of the advanced 3D optical geometry measurement technology. Geometrically mistuned models (GMMs) are semi-automatically constructed upon the precisely measured blisk geometry by an efficient FE mesh updating strategy. They provide explicit, high-fidelity digital representations of the geometric variances within the integrally manufactured blisk. A 'Sector Mode Assembling Reduction Technique' is developed and specifically tailored for efficient dynamic analysis of the large-sized GMMs at a relatively low computational cost and memory requirement. Intensive test campaigns, including forced response tests in the stationary/spinning rig under well-controlled laboratory conditions, are carried out for a full assessment of the GMMs' dynamic prediction capability. Experimental verification results show that the GMM is able to capture the modal dynamics and resonant vibration of the stationary/rotating blisk with satisfactory accuracy. The physical-reality-based GMM converted directly from the precise geometry measurement data can be considered as a viable and valuable tool for predictive vibration evaluation of blisks. However, its model accuracy exhibits a mode-related dependence on the mesh density. The tradeoff between model accuracy and prohibitive computational cost proved to be the bottleneck of this promising blisk modeling approach.

Preprint submitted to Mechanical Systems and Signal Processing *October 3, 2023*

Keywords: blisks, geometric variances, finite element modeling, model reduction, forced response tests

1. Introduction

Driven by the continuing demand for high aero-engine performance and reduced weight, modern fan/compressor designs tend to utilize the integral bladed disks (blisks), instead of the traditional inserted-blade designs. The increasing blade loading, in conjunction with negligible mechanical damping of blisks result in high susceptibility to blade vibration problems. In addition, there are always random, inevitable geometry variances among the blades within blisks, which is referred as geometric mistuning. Even though geometric mistuning is typically small due to the narrow manufacturing tolerances of modern blisks, it has a profound effect on the system dynamics of blisks. Mode localization phenomenon and excessive blade vibration level are commonly observed for the blisks under rig/engine tests. The impact of blade geometric variances on the structural dynamics of bladed disks has been raising continuous and living research interest [1, 2, 3, 4, 5, 6].

In early times, researchers attempted to measure the blade geometry by using a coordinates measurement machine with the aim of extracting the 'blade-alone' vibratory parameters from the measured geometry data [7]. The principal component (PC) analysis or proper orthogonal decomposition (POD) [8] allows to capture the geometry variances of a group of blades by quite a few PCs or POD features.

The past decade has seen the increasing applications of the advanced 3D optical geometry measurement technology in order to fully capture the small blade geometry variances with high precision [9, 10, 11, 12]. A Geometrically Mistuned Model (GMM), or the so-called 'as-manufactured model', could be further constructed upon the precisely measured geometry of a given blisk [13, 14]. The resultant GMM is therefore able to represent the geometric mistuning with high fidelity. Generally, geometric mistuning is considered to cause simultaneous perturbations in the mass and stiffness matrices associated with each individual blade, which further alter both the 'blade-alone' frequencies and mode shapes. The latter, however, is absent in the traditional frequency-mistuning modeling approach for blisks [15, 16], which assumes the deviation of 'blade-alone' frequencies from the nominal design as the unique blade mistuning source. Benefiting from the improved geometric mistuning modeling capability, potential applications of the GMMs, i.e. accurate digital replicas of the physical reality, for predicting the real blisks' dynamics are growing [17, 18]. In addition, they can also be utilized for optimization of sensor placement in the rotating blisks [19, 20, 21], and accurate aeroelastic

simulations [22, 23], etc.

The computational efficiency problem arising from the dynamic analysis of the large-scale, high-fidelity GMMs is of primary concern in practice. Different model reduction techniques can be employed in order to avoid the computationally expensive, full-blisk GMM simulations. Depending on whether a dynamic substructuring step is involved or not, these reduction techniques can be basically divided into two groups: (1) the component-mode-based methods that stem from the technique of component mode synthesis, and require to partition the full blisk GMM into either blade/disk components [24] or sector components [25, 26]; (2) the system-mode-based methods that construct the reduction mode basis by collecting the truncated cyclic modes of the different geometrically mistuned sectors [27, 28, 29]. In brief, the component-mode-based methods are well suited for the general geometrically mistuned blisks. But they also suffer a large number of component interface degree-of-freedoms (DOFs) retained in the reduced-order model and the cost-ineffective constraint mode computations [30]. While the system-mode-based methods are in general more computationally efficient, their applicability scope is confined to the small geometric mistuning with topological compatible meshes over all the blades.

Prior to being used for monitoring and forecasting the blisk's structural performance, the GMMs must undergo the process of model verification and validation. Nevertheless, the experimental verification of the GMMs' dynamic prediction capability has been also facing a big challenge. The key point is to formulate the appropriate verification scenarios to evaluate to what degree the GMMs can reproduce the experimental observations. In the preceding research efforts, it was common to compare the blade geometric mistuning evaluation results by the GMMs with the experimentally identified blade frequency mistuning patterns in the real blisks [13, 31, 32, 33]. As a matter of fact, due to the high sensitivity of the blisk dynamics to blade geometric variances, a full assessment of the GMMs can only be achieved by forced response tests for the blisk under typical engine order excitation. Recent research works attempted to compare the forced response variations predicted by the GMMs with the experimental measurements during the bench/rig tests [34, 35]. Nevertheless, due to the modeling assumptions and limitations introduced by the GMM, and the unavoidable uncertainties in the experimental campaigns on bench/rig tests, correlation between the GMM predictions and the experimental counterparts could not be completely satisfactory.

This paper addresses the methodological development of predictive dynamic modeling and analysis of integral bladed disks through digital representations constructed upon high-precision optical geometry measurements. Specifically, high-fidelity geometrically mistuned models (GMMs) of an integrally manufactured blisk test piece will be semi-automatically constructed by employing the state-of-the-art 3D optical geometry scanning technology. The GMMs are proceeded by a "Sector Mode Assembling Reduction Technique" (SMART), to reduce its model size and computational cost. The prototype of the SMART approach, purposely developed by the authors of this paper for blisks with blend repairs and small mistuning, proved to outperform the aforementioned component-mode-based/system-mode-based methods [36]. In this paper, it will be further developed and specifically tailored for efficient dynamic analysis of the large-sized GMMs with a significant reduction of memory requirement. A variety of test campaigns, particularly the forced response tests in the stationary/spinning test rig under well-controlled laboratory conditions, are organized to experimentally verify the predictive performance of the GMMs. Above all, the objective of this research is to obtain an in-depth and comprehensive understanding of the technical challenges and the capability of the emerging geometric-mistuning modeling approach for blisks.

This paper is organized as follows. The methodologies for the GMM construction and dynamic analysis of the GMM are elaborated in Sec. 2. The GMM is verified against the blade mistuning experimentally evaluated by a recently developed mistuning identification technique based on blade detuning tests [37], as well as the full-blisk modal test data in Sec. 3. The blisk is then subjected to forced response tests in a stationary traveling wave excitation test rig, where the engine order excitation typically occurring in the aero-engine can be simulated in a cost-effective way. This test campaign allows for a first validation of the forced response predictions by the GMM at non-rotating conditions. Subsequently, a second forced response test campaign is performed in a spinning rig. The non-intrusive blade tip-timing technique (BTT) is adopted to measure the vibration of all the individual rotating blades. Prediction capabilities of the GMM are fully assessed and verified in Sec. 4.

2. Methodology

Fig. 1a shows the integrally manufactured blisk test piece mounted onto a stationary traveling wave excitation test rig, which will be described later on. The blisk is made of steel with nickel plated, and consists of $N = 12$ nominally identical sectors with simplified geometric shape. The disk center is clamped by bolts with controlled torque. In the nominal finite element sector model presented in Fig. 1b, the detailed geometry features around the center are neglected for simplicity.

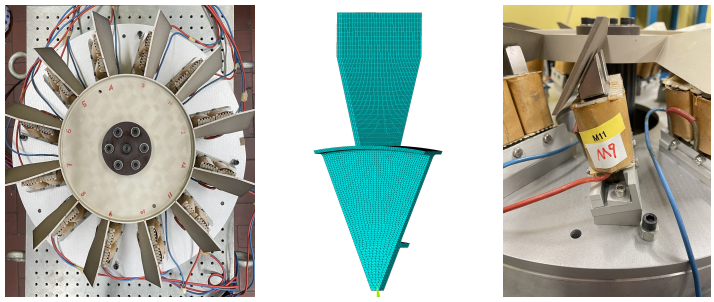

(a) (b) (c)

Figure 1: Simplified blisk test piece mounted on a traveling wave excitation test rig: (a) blisk structure; (b) nominal sector model; (c) an electromagnetic unit.

The dynamic characteristics of the blisk in its nominal design are represented by the numerical frequency vs nodal diameter diagram in Fig. 2. This research focuses on the 1st and 3rd mode family in Fig. 2, which correspond to the first bending (1B) and first torsional (1T) blade-dominated mode family, respectively. The 2nd mode family is not of interest because it is a typical disk-dominant family.

The forthcoming subsections present the methodologies of constructing the geometrically mistuned model and dynamic analysis for the blisk under investigation.

2.1. GMM Construction

Blade-to-blade geometry variances within the blisk test piece is due to the manufacturing tolerance. A Geometrically Mistuned Model (GMM), of the blisk is constructed by exploiting the non-contact Advanced TOpometric Sensor (ATOS) structured-blue-light 3D scanner. This optical scanner

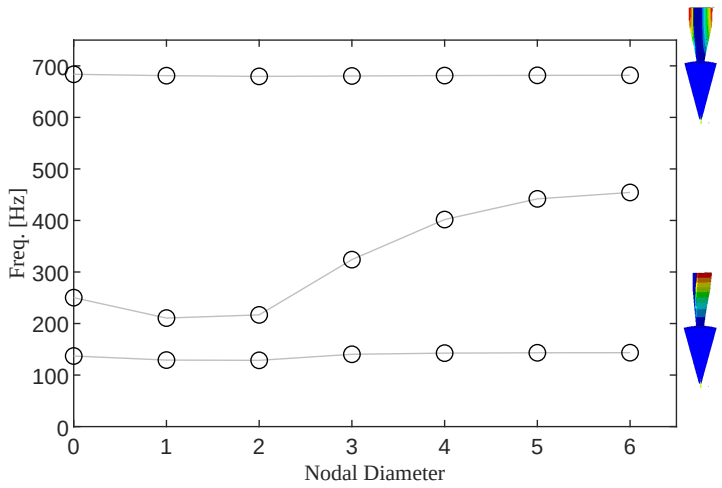

Figure 2: Frequency vs nodal diameter diagram with Coupling indices in percentage.

provides full-field precision scans of the blisk surface with allowable high resolutions down to 2.5 μm. It has been proved that the ATOS series of industrial 3D scanner is able to capture the blade-to-blade geometry variances within industrial blisks with satisfactory accuracy [10].

As shown in Fig. 3(a), the blisk at rest firstly undergoes a number of fringe projection scans that enable to precisely acquire the full blisk geometry data in the form of an accurate and dense point cloud. The blisk point cloud is then tessellated into triangulated surface meshes presented in Fig. 3(b). Historically, a detailed finite element model (FEM) can be constructed by the classical reverse engineering method [38]. Namely, the point cloud is firstly processed into a solid CAD model, and then meshed into a FEM. Nevertheless, the whole process requires a labor-intensive effort.

In this research, a GMM is semi-automatically constructed by correlating an existing 'seed' FEM directly with the point cloud representing the measured blisk geometry. The seed FEM with quadratic tetrahedral volume elements is considered as an initial approximation of the real blisk with blade geometry variances. The tuned blisk model in the nominal design is widely considered a good candidate for the seed FEM. A dedicated mesh updating strategy is then applied to automatically modify the surface node coordinates of the seed FEM in order to match the point cloud as much as possible. The interior volume mesh of the seed FEM is regenerated according

to the updated surface mesh, which eventually gives rise to the GMM. More details about this mesh updating strategy can be found in the authors' recent research work [39].

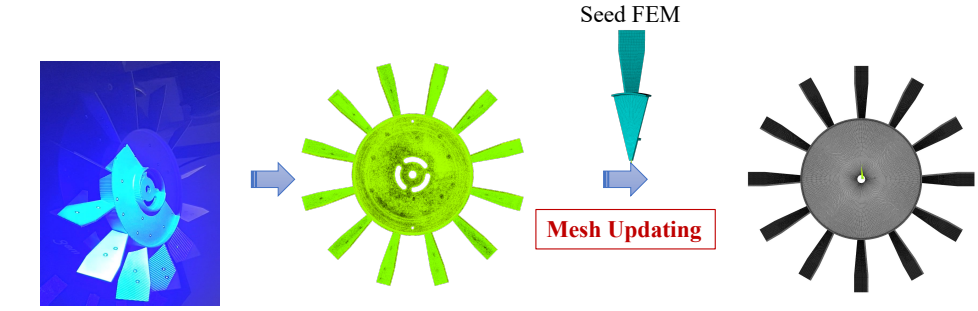

Figure 3: Construction of the GMM.

The resultant GMM is characterized by a morphed mesh that enable to explicitly model the detailed blisk surface geometry features. This is proved by examining the surface node to point cloud distance for the seed FEM before mesh updating and afterwards. Fig. 4 shows that the average seed FEM surface node to point cloud distance at blade 1 is reduced from 110μm to 0.02μm with the mesh updating. It demonstrates that the GMM is able to represent the measured blisk geometry with high fidelity.

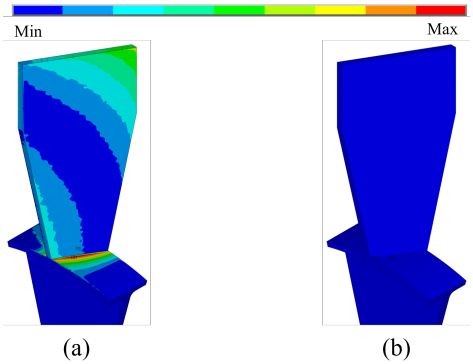

Figure 4: Surface FEM node to point cloud distance at blade 1: (a) before mesh updating; (b) after mesh updating.

It has been reported that blisk FEMs built upon the precisely measured geometry usually require high mesh density to fully capture the frequency/mode variations due to blade geometric variances [40]. In this research, influence of mesh density on the performance of GMM will be investigated in Sec. 3. To this end, two GMMs are constructed from a seed blisk FEM with normal and high mesh density, respectively. The high mesh-density GMM naturally raises major concern over its computational cost and efficiency. Apart from the prohibitive computational time consumption for the full-blisk simulations, the high memory requirement is also a major bottleneck since it determines the allowable model size of GMM. This issue is fully addressed in the next subsection.

2.2. Dynamic Analysis

The full-blisk GMMs, of which the dynamic analyses are generally computationally expensive, are proceeded into reduced-order models (ROMs) by the Sector Mode Assembling Reduction Technique. Originally developed by the authors of this paper for the blisks in the presence of both small geometric mistuning and large blends [36], the SMART approach is further developed and specifically tailored in this research for efficient dynamic analysis of the high mesh-density, large-sized GMM. As conceptually illustrated in Fig. 5, it starts from the equation of motion of the full-order GMM written in a "uncoupled" form:

$$\bar{\mathbf{M}}\ddot{\bar{\mathbf{x}}} + (\bar{\mathbf{C}} + \bar{\mathbf{G}})\dot{\bar{\mathbf{x}}} + \bar{\mathbf{K}}\bar{\mathbf{x}} = \bar{\mathbf{f}} \tag{1}$$

where the full-blisk displacement vector $\bar{\mathbf{x}}$ is comprised of the sector-level displacement vectors of all the N individual sectors as $\bar{\mathbf{x}} = [\bar{\mathbf{x}}_1; \bar{\mathbf{x}}_2; \cdots \bar{\mathbf{x}}_N]^{\mathrm{T}}$. The "bar" notation denotes sector-level quantities throughout this paper. These quantities include the interior DOFs (I) and redundant DOFs related to the cyclic interfaces (Γ) of each sector. For instance, according to the notation for the j^{th} sector, the sector-level displacement vector is written as $\bar{\mathbf{x}}_j = [\mathbf{x}_{j,\mathrm{I}}; \mathbf{x}_{j,\Gamma}]^{\mathrm{T}}$. Accordingly, the sector-level mass matrix in the local cylindrical coordinate system associated with each sector are gathered to form the full-blisk mass matrix as $\bar{\mathbf{M}} = \mathrm{blkdiag}(\bar{\mathbf{M}}_1, \bar{\mathbf{M}}_2, \cdots, \bar{\mathbf{M}}_N)$. The other full-blisk system quantities, i.e. the stiffness matrix $\bar{\mathbf{K}}$, the symmetric damping matrix $\bar{\mathbf{C}}$, the skew-symmetric gyroscopic matrix $\bar{\mathbf{G}}$ and the excitation force $\bar{\mathbf{f}}$, are formed in a similar manner.

The basic idea of the SMART approach is to substructure the full blisk GMM into N physically "isolated" sectors. Physical displacement of each

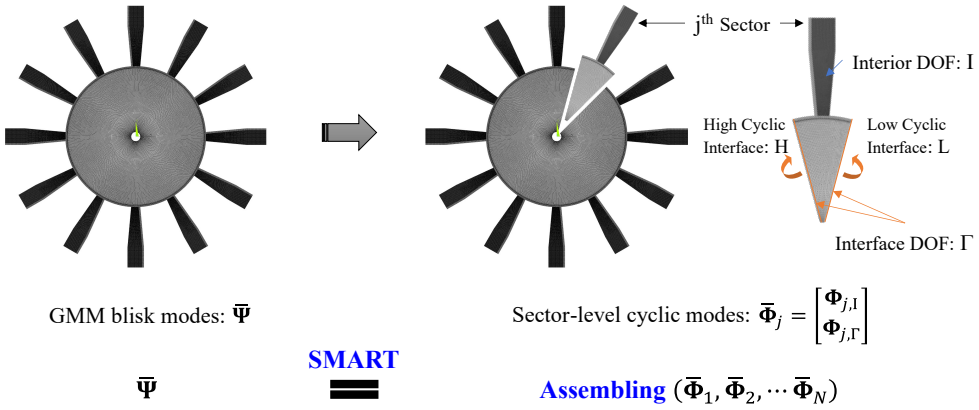

Figure 5: Schematic diagram of the SMART approach.

sector $\bar{\mathbf{x}}_j$, with a unique geometric profile, is independently approximated by a set of n_m truncated cyclic modes of its own:

$$\bar{\mathbf{x}}_j = \begin{bmatrix} \mathbf{x}_{j,\mathrm{I}} \\ \mathbf{x}_{j,\Gamma} \end{bmatrix} = \begin{bmatrix} \mathbf{\Phi}_{j,\mathrm{I}} \\ \mathbf{\Phi}_{j,\Gamma} \end{bmatrix} \mathbf{q}_j = \bar{\mathbf{\Phi}}_j \mathbf{q}_j, \quad j = 1, 2, \cdots, N \tag{2}$$

where $\bar{\mathbf{\Phi}}_j$ denotes the retained complex-valued cyclic modes of the j^{th} sector with assumed cyclic symmetry at the sector interfaces Γ; $\mathbf{q}_j$ representing the modal contribution is to be determined.

The SMART approach exploits the similitude observed between the modal deflections restricted to the disk part in the cyclic modes for the 1^{st} and j^{th} sector, respectively. Hence, $\mathbf{\Phi}_{1,\Gamma}$ can be expressed as a weighted sum of the interface modes $\mathbf{\Phi}_{j,\Gamma}$ of the j^{th} sector, by means of an Interface Mode Transformation (IMT):

$$\mathbf{\Phi}_{j,\Gamma} \mathbf{T}_{\gamma,j} = \mathbf{\Phi}_{1,\Gamma}, \quad j = 1, 2, \cdots, N \tag{3}$$

where $\mathbf{T}_{\gamma,j}$ denotes the transformation matrix of the size $n_m \times n_m$ for the j^{th} sector. It can be readily approximated as a least-square solution to Eq. (3) at a negligible computational cost. In particular, $\mathbf{T}_{\gamma,1}$ is an identity matrix for the reference sector 1. With the introduction of IMT matrix $\mathbf{T}_{\gamma,j}$, the sector-level mode projection presented in Eq. (2) evolves into the form below:

$$\bar{\mathbf{x}}_j = \bar{\mathbf{\Phi}}_j \mathbf{T}_{\gamma,j} \mathbf{q}_j = \begin{bmatrix} \mathbf{\Phi}_{j,\mathrm{I}} \\ \mathbf{\Phi}_{j,\Gamma} \end{bmatrix} \mathbf{T}_{\gamma,j} \mathbf{q}_j = \begin{bmatrix} \mathbf{\Phi}_{j,\mathrm{I}} \mathbf{T}_{\gamma,j} \\ \mathbf{\Phi}_{1,\Gamma} \end{bmatrix} \mathbf{q}_j, \quad j = 1, 2, \cdots, N \tag{4}$$

Note that Eq. (4) naturally holds because it merely represents a linear transform of the projection basis. The modal coordinates $\mathbf{q}_j$ to be determined also evolves accordingly. At this point, the new mode basis for the j^{th} sector carries the same modal information at the disk interface DOFs by $\mathbf{\Phi}_{1,\Gamma}$ as that of the reference sector 1. Meanwhile, the modal characteristics pertained to the j^{th} sector are fully preserved as $\mathbf{\Phi}_{j,\text{I}}\mathbf{T}_{\gamma,j}$.

Subsequently the new mode basis of all the separate sectors are strategically assembled to form the reduction mode basis for the full blisk. A physical displacement compatibility condition is imposed to ensure the displacement continuity at the common disk interface between the adjacent sectors. Namely, the displacement at the high cyclic interface of the j^{th} sector should be consistent with that at the low cyclic interface of the $(j+1)^{\text{th}}$ sector

$$\bar{\mathbf{x}}_{j,\text{H}} = \bar{\mathbf{x}}_{j+1,\text{L}}, \quad j = 1, 2, \cdots, N \tag{5}$$

where the right-hand side should be replaced by $\bar{\mathbf{x}}_{1,\text{L}}$ if $j = N$.

After some simple algebraic manipulations, the dependence between the modal coordinates for two adjacent sectors can be derived from Eq. (4) and (5):

$$\mathbf{T}(\alpha)\mathbf{q}_j = \mathbf{q}_{j+1}, \quad j = 1, 2, \cdots, N-1 \tag{6}$$

where $\mathbf{T}(\alpha)$ is a block diagonal matrix linking the cyclic modes at the low/high cyclic interface DOFs in $\mathbf{\Phi}_{1,\Gamma}$, i.e. $\mathbf{\Phi}_{1,\text{H}} = \mathbf{\Phi}_{1,\text{L}}\mathbf{T}(\alpha)$. Simply, it can be analytically constructed as a function of the fundamental inter-blade phase angle $\alpha = 2\pi/N$:

$$\mathbf{T}(\alpha) = \text{blkdiag}(\mathbf{I}_{n_m^{(0)}}, e^{i\alpha} \otimes \mathbf{I}_{n_m^{(1)}}, \cdots, e^{ih\alpha} \otimes \mathbf{I}_{n_m^{(h)}}, \cdots) \tag{7}$$

where $\mathbf{I}_{n_m^{(h)}}$ is an identity matrix of the size $n_m^{(h)}$, which is the number of retained cyclic modes with the harmonic index h.

Substituting Eq. (6) into Eq. (4) leads to the sector-level mode projection in the final form:

$$\bar{\mathbf{x}}_j = \bar{\mathbf{\Phi}}_j\mathbf{T}_{\gamma,j}\mathbf{T}[(j-1)\alpha]\mathbf{q}_1 = \bar{\mathbf{\Psi}}_j\mathbf{q}_1, \quad j = 1, 2, \cdots, N \tag{8}$$

where the SMART reduction mode basis for the j^{th} sector reads $\bar{\mathbf{\Psi}}_j = \bar{\mathbf{\Phi}}_j\mathbf{T}_{\gamma,j}\mathbf{T}[(j-1)\alpha]$. $\mathbf{q}_1$ becomes the one and only retained generalized coordinates to be determined.

The SMART reduction mode basis for the full blisk takes the form of $\bar{\mathbf{\Psi}} = \left[\bar{\mathbf{\Psi}}_1; \bar{\mathbf{\Psi}}_2; \cdots \bar{\mathbf{\Psi}}_N\right]^{\text{T}}$. By substituting Eq. (8) into Eq. (1) and premultiplying

by $\bar{\mathbf{\Psi}}^{\mathrm{H}}$, the equation of motion of the full-order GMM can be reduced in terms of the generalized coordinates $\mathbf{q}_1$:

$$\mathbf{M}_{\mathrm{red}}\ddot{\mathbf{q}}_1 + (\mathbf{C}_{\mathrm{red}} + \mathbf{G}_{\mathrm{red}})\dot{\mathbf{q}}_1 + \mathbf{K}_{\mathrm{red}}\mathbf{q}_1 = \mathbf{f}_{\mathrm{red}} \tag{9}$$

Benefiting from the block structure of the SMART reduction mode basis, the reduced system quantities can be obtained by the sector-level computations with a relatively low memory requirement:

$$\mathbf{M}_{\mathrm{red}} = \bar{\mathbf{\Psi}}^{\mathrm{H}}\bar{\mathbf{M}}\bar{\mathbf{\Psi}} = \textstyle\sum_{j=1}^{N} \bar{\mathbf{\Psi}}_j^{\mathrm{H}}\bar{\mathbf{M}}_j\bar{\mathbf{\Psi}}_j \tag{10}$$

$$\mathbf{C}_{\mathrm{red}} = \bar{\mathbf{\Psi}}^{\mathrm{H}}\bar{\mathbf{C}}\bar{\mathbf{\Psi}} = \textstyle\sum_{j=1}^{N} \bar{\mathbf{\Psi}}_j^{\mathrm{H}}\bar{\mathbf{C}}_j\bar{\mathbf{\Psi}}_j \tag{11}$$

$$\mathbf{G}_{\mathrm{red}} = \bar{\mathbf{\Psi}}^{\mathrm{H}}\bar{\mathbf{G}}\bar{\mathbf{\Psi}} = \textstyle\sum_{j=1}^{N} \bar{\mathbf{\Psi}}_j^{\mathrm{H}}\bar{\mathbf{G}}_j\bar{\mathbf{\Psi}}_j \tag{12}$$

$$\mathbf{K}_{\mathrm{red}} = \bar{\mathbf{\Psi}}^{\mathrm{H}}\bar{\mathbf{K}}\bar{\mathbf{\Psi}} = \textstyle\sum_{j=1}^{N} \bar{\mathbf{\Psi}}_j^{\mathrm{H}}\bar{\mathbf{K}}_j\bar{\mathbf{\Psi}}_j \tag{13}$$

$$\mathbf{f}_{\mathrm{red}} = \bar{\mathbf{\Psi}}^{\mathrm{H}}\bar{\mathbf{f}} = \textstyle\sum_{j=1}^{N} \bar{\mathbf{\Psi}}_j^{\mathrm{H}}\bar{\mathbf{f}}_j \tag{14}$$

In the implementation practice, the projection process above is efficiently realized by managing the single-sector matrix and modes in a sector-by-sector manner, rather than by loading all the N-sector quantities into the memory simultaneously.

Eq. (9) represents a SMART ROM, whose size is determined by the number of retained cyclic modes n_m for each individual sector. Notice that in fact, the modal characteristics pertained to each geometrically mistuned sector are fully involved in the SMART reduction mode basis. It thus ensures that the SMART ROM is able to reproduce the dynamics of the full-order GMM with high accuracy.

Overall, the full blisk GMM mode computation boils down to N individual sector analysis, which is independently proceeded for the cyclic modes of each sector with assumed cyclic symmetry at the sector interfaces. The latter also gives a favorable condition for the derivation of ROM by the sector-level projection. Hence, the SMART approach specifically tailored in this research enables to carry out dynamic analysis of the GMM with a huge reduction of memory usage, compared with the full-order GMM simulation. More importantly, in case of a limited amount of physical memory, the maximum allowable size of the GMM can be enlarged by the SMART approach.

The SMART approach possesses multiple advantages over the existing model reduction techniques already mentioned before. In particular, the 'substructuring' step enables the SMART approach to deal with small sector-level geometric variances, as well as the large blade geometric modification

due to material loss, blade repair, etc. Nevertheless, it is exempted from the cost-ineffective constrain mode computations, which are required by the classical component-mode-based methods. In addition, no component interface DOFs are retained in the final SMART ROM.

2.3. Geometric Mistuning Evaluation

The GMM allows to perform the geometric mistuning evaluation in a straightforward manner. As for the blisk test piece, Fig. 4(a) shows that the maximum geometry deviation generally occurs around the fillet area at the blade-disk interfaces. Hence, the sector frequency variations due to the sector-level geometry non-uniformity are computed to measure the geometric mistuning. Note that the sector frequencies are already available as the by-product of the independently proceeded cyclic modal analyses during the SMART application. The fractional shift in terms of the cyclic mode frequency $f_{j,m}$ of the j^{th} sector at the median nodal diameter of the m-th mode family is calculated as the sector frequency variation:

$$ {}^{\text{S}}\delta_{j,m}^{\text{GMM}} = \frac{f_{j,m} - \bar{f}_m}{\bar{f}_m}, \quad j = 1, 2, \cdots, N \tag{15} $$

where the preceding superscript ${}^{\text{S}}(\cdot)$ indicates a sector frequency variation; $\bar{f}_m$ is the mean value of $f_{j,m}$ with $j = 1, \cdots, N$.

It should be reminded that geometric mistuning usually causes simultaneous variations in both the sector frequencies and mode shapes (of the blade part in particular). The quantification of the mode shape variations is not considered in this research. The impact of geometric mistuning on the global blisk dynamics will be assessed in the next section.

3. Model Verification

The geometrically mistuned blisk model previously presented will be verified against the experimental data of the blisk mounted in a stationary traveling wave excitation test rig. Capability of the GMM in: (1) capturing the sector frequency variations within the real blisk structure; (2) reproducing the full-blisk modal dynamics, will be assessed. To this end, different vibration tests (see Fig. 6) are performed and briefly described below. The following subsections present the model verification results for the GMM with normal and high mesh density, respectively.

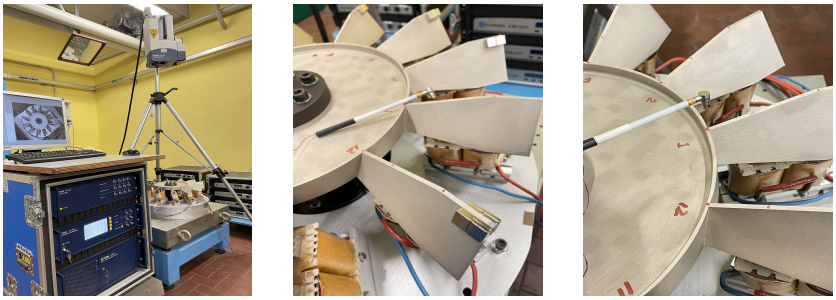

(a) (b) (c)

Figure 6: Vibration tests for the blisk clamped onto a stationary traveling wave excitation test rig: (a) test setup; (b) blade detuning test; (c) modal test.

3.1. Vibration Tests

Two different hammer tests are carried out for the purpose of experimentally evaluating the frequency mistuning patterns and the full-blisk modal properties, respectively.

- Experimental mistuning evaluation based on blade detuning tests

The 'blade-alone' frequency mistuning pattern of the real blisk is experimentally evaluated by a recently developed mistuning identification technique based on blade detuning tests (BDTID) [37]. It consists of blade detuning tests followed by a correction procedure. The detuning tests enable to approximately evaluate the 'blade-alone' frequencies through blade-by-blade impact testing in combination with a mass detuning mechanism. As shown in Fig. 6b, identical detuning masses (8 squared magnets with a total weight of 14g) are attached onto all the blades at the same position, except the one currently under test. A miniature instrumented hammer is used to impulsively excite the blade without detuning mass. A single test FRF is acquired with the response measurement at the blade tip by the non-contact Laser Doppler vibrometer (LDV). Since the inherent inter-blade coupling within the blisk is largely suppressed by the detuning masses, an isolated peak with the highest magnitude is manifested in the test FRF as a m-th blade-alone mode. Subsequently, the correction procedure takes into account the residual inter-blade coupling and gives more accurate blade-alone mistuning evaluation results. In a parallel research, the BDTID technique proves to be able

to capture the 'true' blade mistuning actually present in the blisk with high reliability.

Furthermore, the experimentally identified blade-alone frequency mistuning value ${}^{\mathrm{B}}\delta_{j,m}^{\mathrm{BDTID}}$ can be transformed into an equivalent sector frequency variation ${}^{\mathrm{S}}\delta_{j,m}^{\mathrm{BDTID}}$. This is realized by simply scaling the blade-alone frequency variation at the j^{th} sector, i.e.

$$ {}^{\mathrm{S}}\delta_{j,m}^{\mathrm{BDTID}} = {}^{\mathrm{B}}\delta_{j,m}^{\mathrm{BDTID}}/\lambda \tag{16} $$

where λ is the fraction of strain energy in the blade for the cyclic mode at the median nodal diameter.

The equivalent sector frequency variations derived by BDTID will facilitate the like-for-like comparison with that evaluated by the GMM according to Eq. (15).

- Modal test

As shown in Fig. 6c, a standard single-input modal test is carried out by employing the miniature hammer impulsively exciting the blisk at the disk rim. The vibration response is measured by the LDV at a tip point of each individual blade. In practice, however, it could be technically difficult to fully extract the mistuned blisk modes from the modal test FRFs with a tight group of nearly repeated modal frequencies. In order to capture the mistuned blisk frequencies and mode shapes as accurate as possible, precautions are taken to ensure the sufficient frequency resolution of the measured FRFs, the well-selected and consistent impulsive excitation point [41]. In this research, all the mistuned blisk modes ($N = 12$ modes associated with the target 1B and 1T mode family, respectively) are successfully extracted from the modal test FRFs by the PolyMax algorithm in the Test.Lab software. The mistuned blisk frequencies and one-point-per-blade mode shapes will serve as experimental reference data for the modal verification of the GMMs.

3.2. Verification of GMM with Normal Mesh Density

The GMM with normal mesh density is composed of about 1.5×10^6 quadratic tetrahedral elements with approximately 2.4×10^6 nodes. Appropriate constraints are imposed onto the nodes in the disk center to represent the clamping boundary condition. Dynamic analysis is then performed in a workstation with 10 cores @1.9 GHz and 64 GB of memory. The experimentally evaluated sector frequency variations based on blade detuning

tests $\boldsymbol{\delta}_m^{\mathrm{BDTID}}$ for the m-th blade mode, and the numerically predicted sector frequency variations based on the GMM with normal mesh density $\boldsymbol{\delta}_m^{\mathrm{GMM}}$, are compared in Fig. 7. It can be seen that the sector frequency mistuning magnitudes fall in a narrow band of $[-1\%, 1.6\%]$. The Pearson correlation coefficient R is then computed to quantify the consistency between the experimentally evaluated/GMM-predicted sector mistuning patterns. Its value is expected to be greater than 0. Values of R close to 1 denote high consistency. Overall, the numerically derived sector frequency mistuning patterns manifest a similar trend with the experimental references ($R = 0.877$ for the 1B mode and $R = 0.845$ for the 1T mode). It is thus inferred that the non-uniform sector geometry variances is the main source of mistuning within the blisk under investigation.

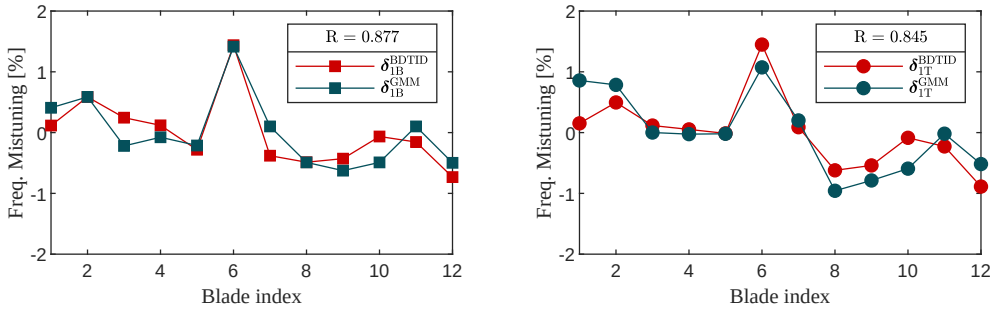

Figure 7: Verification of sector frequency mistuning patterns evaluated by the normal mesh-density GMM: (a) 1B mode; (b) 1T mode.

Subsequently, modal correlation by the Modal Assurance Criterion Analysis (MAC) is carried out to quantify the discrepancy between the experimental reference data and the GMM-predicted data sets. It can be seen in Fig. 8a that for the majority of blade-dominated modes of the 1B mode family, the blisk modal properties numerical computed by GMM are generally in good agreement with the experimental reference data. Exception comes at mode $1 \sim 4$ with obvious modal discrepancies. This is owing to the non-ideal clamping boundary conditions in the disk center. Note that these 4 modes correspond to the split modes of the tuned blisk at ND1$\sim$2, which tends to behave as disk-dominant modes (see Fig. 2). Consequently, the relatively high disk participation in the blisk modes renders them affected by the disk

clamping uncertainties to a considerable extent. The overall good modal correlation for 1B mode family confirms that the prevailing blade mistuning stems from blade geometry variations due to the manufacture tolerance.

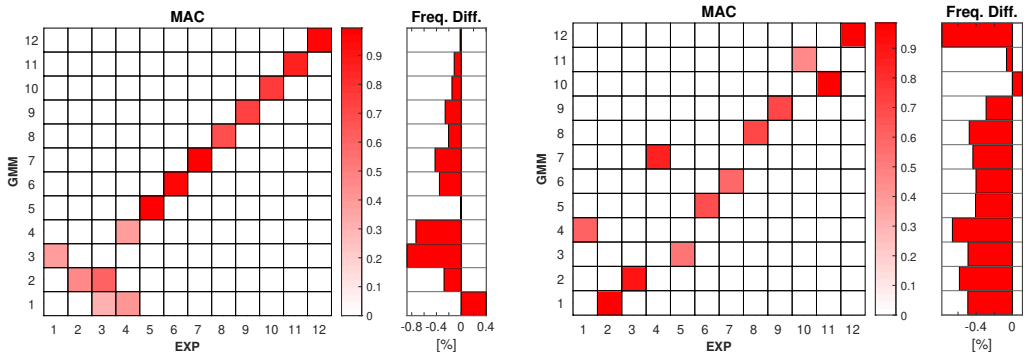

Figure 8: Modal correlation between experimental reference data and numerically predicted data by the normal mesh-density GMM: (a) 1B mode family; (b) 1T mode family.

On the contrary, correlation between the experimental/numerically derived full-blisk modes of 1T family is not good enough since the MAC matrix in Fig. 8b shows a number of off-diagonal terms. An improved modal correlation for 1T mode family will be found with the GMM with higher mesh density.

3.3. Verification of GMM with High Mesh Density

In order to more accurately capture the blisk mode variations due to geometric variance, the blade and disk rim meshes of the seed FEM are refined during the GMM construction. Thanks to the model reduction technique of SMART, the GMM with high mesh density comprising about 6.6×10^6 quadratic tetrahedral elements is still within the capacity, but close to the limit of the available memory in the work station.

Fig. 9 reveals that the increased mesh density brings about the sector frequency mistuning patterns with slightly higher consistency with respect to the experimental evaluations ($R = 0.881$ for the 1B mode and $R = 0.877$ for the 1T mode). It should be reminded that the experimental mistuning evaluation based on blade detuning tests is derived from the traditional frequency-mistuning modeling approach of blisks. It assumes that all the mistuning is uniquely represented in the form of blade-alone frequency/elastic

modulus variations, regardless of the physical mistuning sources within the blisk structure under investigation. While as remarked earlier, the sector frequency variation predicted by the GMM according to Eq. (15) only partly represents the impact of geometric variance on the sector-level dynamics. Hence, the remaining discrepancy observed in Fig. 9 is probably due to the different modeling assumptions involved in the derivation of the experimentally evaluated/GMM-predicted frequency mistuning patterns.

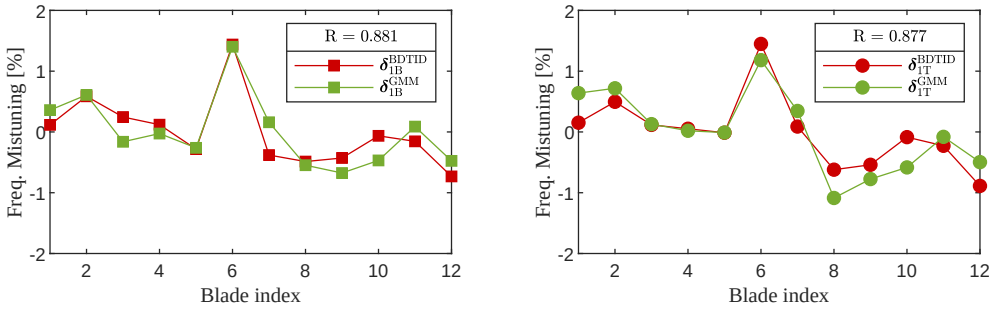

Figure 9: Verification of sector frequency mistuning patterns evaluated by the high mesh-density GMM: (a) 1B mode; (b) 1T mode.

In addition, this high mesh-density GMM gives rise to good modal correlation results for 1B mode family (see Fig. 10a) consistent with the previous GMM with normal mesh density. More importantly, an overall improved mode shape correlation can be clearly seen in the MAC plot for 1T mode family in Fig. 10b. Apart from those minor discrepancies limited to a few modes, it can be stated that the GMM with high mesh density capture the modal behaviors of the blisk with acceptable accuracy.

At this point, it appears more reasonable to verify the GMM against the full-blisk modal test data, rather than against the experimentally determined frequency mistuning patterns. Moreover, it is also clarified that the mesh density has a mode-dependent effect on the accuracy of the high-fidelity blisk model built upon the measured geometry. A trade-off between the model accuracy and the computational cost, which escalates sharply with the increasing mesh density, has to be taken into consideration. For this reason, the GMM with further refined blade meshes is not investigated in

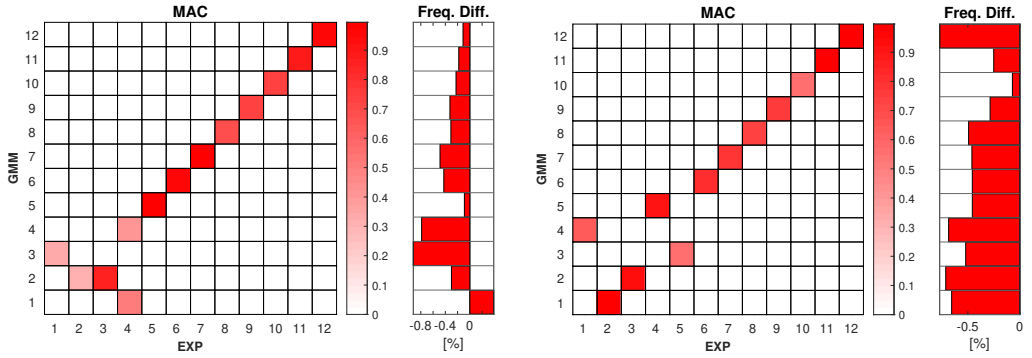

Figure 10: Modal correlation between experimental reference data and numerically reconstructed data by GMM with high mesh density: (a) 1B mode family; (b) 1T mode family.

this research. In the forthcoming section, the GMM with high mesh density will be validated against the forced response test data.

4. Forced Response Tests and Model Validation

In this section, the blisk test piece firstly undergoes forced response tests in a stationary traveling wave excitation (TWE) test rig. It allows to validate the forced response predictions by the GMM at non-rotating conditions in a cost-effective way and with much flexibility in the measurement process. Afterwards, forced response tests are also conducted in a spinning rig under vacuum condition. Predictive performance of the GMM in terms of forced responses under typical engine-order excitation will be validated by a wealth of test data acquired by the non-intrusive blade tip-timing technique.

4.1. Stationary rig tests & model validation

The stationary TWE test rig, which has already been shown in Fig. 1a, is able to simulate the Engine Order (EO) excitation that the actual bladed disks would experience in operation [42, 43]. With a upper frequency limit of 600 Hz, this test rig allows to perform forced response tests in the frequency range covering the 1B mode family of the blisk test piece. This paper presents the forced response tests under a representative EO3 excitation.

The test rig utilizes N cyclically repeated electromagnetic (EM) units (see Fig. 1c) under individual blades to exert a non-contact force onto each

blade simultaneously. Each EM unit is fed by a harmonic input voltage with controlled frequency, amplitude and inter-blade phase shift determined by the EO value. For instance, the EO3 excitation drives the phase shift of $2\pi \times \mathrm{EO}/N = \pi/2$ between adjacent blades. Meanwhile, forced responses of the blisk are measured at the tip of each blade in the axial direction by the LDV.

Fig. 11a depicts the forced response curve at blade 1 computed by the high mesh-density GMM. Due to the mistuning, the tuned blisk mode pair at ND3 of the 1B mode family is split into 2 closely spaced mistuned blisk modes. As expected, the principal resonance peaks signify that a dominant ND3 mode component is strongly excited by the EO3 excitation. Accordingly, the ODS (Operational Deflection Shape) is measured respectively at the resonant frequencies, as presented in Fig. 11(b) and (c). These ODS exhibit modulated spatial wave shapes, a hint of moderate mode localization due to mistuning.

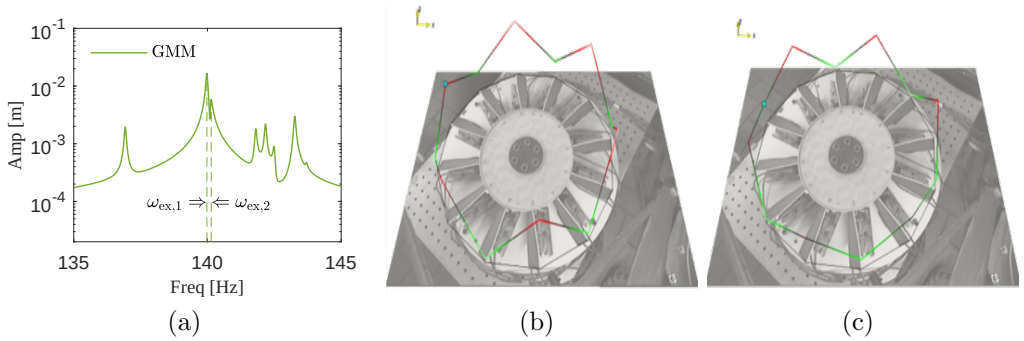

Figure 11: Forced response test in the stationary rig: (a) forced response predicted by GMM at blade 1; (b) Measured ODS at $\omega_{\mathrm{ex},1}$; (c) Measured ODS at $\omega_{\mathrm{ex},2}$.

A correlation analysis is conducted at the peak frequency $\omega_{\mathrm{ex},1}$ (Fig. 12a) and $\omega_{\mathrm{ex},2}$ (Fig. 12b), respectively. Since the excitation force amplitude is not available, the ODS is normalized for comparison so that the maximum blade amplitude is equal to 1. It appears that the ODS predicted by GMM shows high correlation with the tested ODS, as indicated by the MAC value of 0.974 and 0.969 respectively. These encouraging results demonstrate the GMM's capability in predicting the relative blade amplitudes of the real blisk at the resonance of the 1B mode family with a high level of confidence.

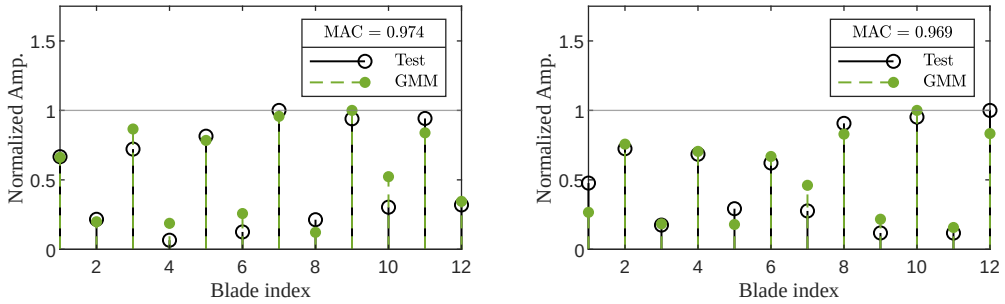

(a) ODS at $\omega_{\mathrm{ex},1}$ (b) ODS at $\omega_{\mathrm{ex},2}$

Figure 12: Comparison of tested/GMM-predicted ODS under an EO3 excitation in the stationary rig test.

4.2. Spinning rig test & model validation

A test campaign is organized in a spinning rig in order to make a complete assessment of the GMM for the forced response prediction of the blisk in a representative, operational environment.

Fig. 13 shows that the blisk test piece is mounted onto the rotating shaft in the vertical direction. The underground test chamber provides vacuum condition during the spinning test. A single magnet is fixed onto a support ring on top of the rotating blisk at an adjustable distance. It produces a non-contact force that each rotating blade feels as a single force impulse during one revolution. The test rig is equipped with the non-intrusive Blade Tip-Timing (BTT) measurement system. In this test campaign, 5 BTT laser sensors are mounted on the support ring at the same distance from the disk center, with the laser beam pointing towards the blade edge at the radius of 190mm. This BTT sensor arrangement is referred as the beam interrupt configuration [44]. It enables to detect the time-of-arrivals of the specified measurement points at the blade edges and further to obtain the vibration displacement in the circumferential direction. The angular positions of the BTT sensors are optimized in order to effectively extract the blade vibration parameters from the acquired measurement data afterwards, including the response order, frequency, amplitudes, phase and damping level, etc. An Once-Per-Revolution (OPR) sensor is also instrumented to provide the timing reference.

The forced response test is carried out by driving the blisk to go across a

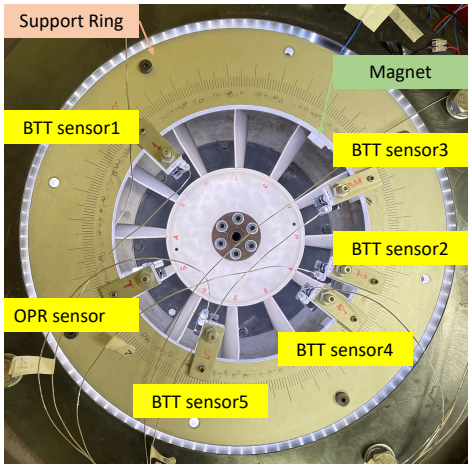

Figure 13: Forced response test in the spinning rig and BTT setup

number of resonances from 600∼3400 rpm at a low sweep rate 0.9375rpm/s. The force applied by the single magnet to the rotating blisk theoretically contains an infinite number of engine order excitation components. Therefore, it turns out that a number of blade-dominated blisk modes could be effectively excited by the single magnet. This paper focuses on two representative resonances observed around 3220rpm and 2050rpm, where the 1B and 1T mode family is excited by an EO3 and EO20 excitation component, respectively.

4.2.1. 1B mode/EO3 resonance

Benefiting from the BTT's all-blade measurement capability, the forced response of all the 12 blades around 3220rpm are depicted in Fig. 14. The forced response curves for the blades of low, median and high resonant magnitudes are highlighted in this plot. It is clearly seen that all the blades reach the highest vibration magnitudes at two slightly different rotation speeds Ω_1 and Ω_2. The underlying reason is that only the split mode pair of the 1B mode family at ND3 are strongly excited by the EO3 excitation component.

In the numerical aspect, the centrifugal effect and the Coriolis effect are included into the GMM at a representative rotation speed 3220rpm. An EO3 excitation with an amplitude of 1 is imposed on the GMM for the forced response simulation. The damping ratio derived from the BTT results serves

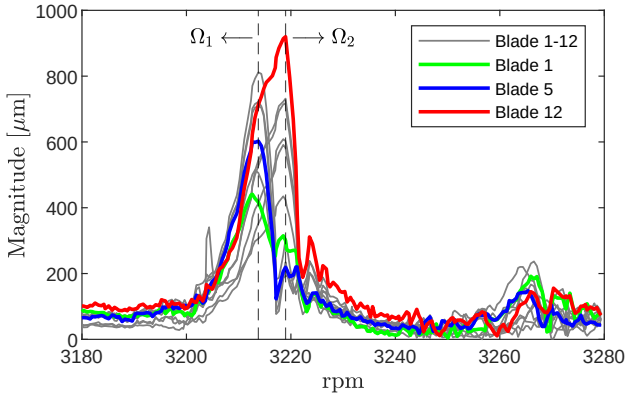

Figure 14: Blade magnitudes versus rotation speed curves by the BTT at 1B mode/EO3 resonance

as the input for the forced response prediction by the GMM.

Both the BTT results and GMM predictions enable to extract the ODS at the resonant speed Ω_1 and Ω_2 respectively. A comparison of the normalized ODS is illustrated in Fig. 15. Once again, the GMM-predicted ODS shows a very similar trend with the ODS measured by the BTT. The MAC values of 0.965 and 0.950 confirm the good correlation between the tested/predicted ODS at the resonant speeds. It is also noticed the blisk ODS measured in the rotational condition in Fig. 15 exhibits considerable deviation from those counterparts measured in the stationary condition, also under an EO3 excitation, in Fig. 12. This highlights the capability of the GMM in capturing the 1B resonant vibration of the rotating blisk with satisfactory accuracy.

4.2.2. 1T mode/EO20 resonance

When it comes to the 1T mode/EO20 resonance, things become different. It appears in Fig. 16 that the resonant speeds of the individual blades scatter in a relatively wider range. This is due to the fact that compared with the 1B mode family, the 1T mode family tends to behave as purely blade-alone modes with less disk contribution. Obviously, all the mistuned blisk modes of the 1T family are strongly excited by the EO20 excitation component. In particular, in the clustered mode region, the forced response of a certain number of blades, e.g. blade 5 in the speed range of 2040∼2060rpm, exhibits multiple peaks owing to the participation of a multitude of mistuned blisk

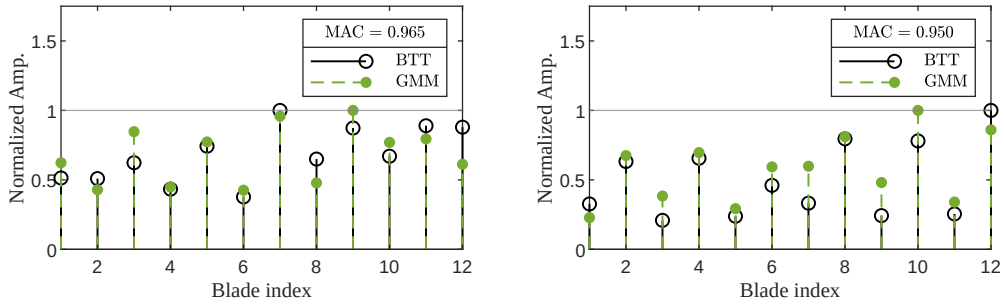

(a) ODS at Ω_1 (b) ODS at Ω_2

Figure 15: Comparison of tested/GMM predicted ODS at 1B mode/EO3 resonance in the spinning rig test.

modes. It is thus difficult to perform the GMM prediction to BTT measurement correlation analysis in this high modal density region. Instead, the measured ODS is extracted for the validation purpose at two selected speeds Ω_3 and Ω_4 respectively, where there appear 'isolated' resonant peaks to some extent.

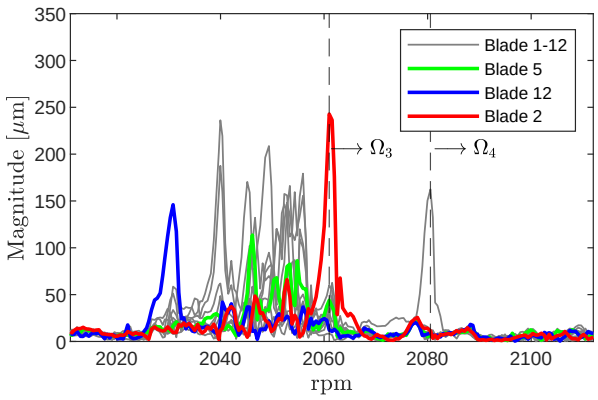

Figure 16: Blade magnitudes versus rotation speed curves by the BTT at 1T mode/EO20 resonance

In general, both the measured ODS at Ω_3 and Ω_4 depicted in Fig. 17 are featured by significant vibration localization phenomenon since a certain

blade possesses a much higher magnitude than all the rest. Basically, the numerically predicted ODS by GMM shows good agreement with the measured ones by BTT, particular at Ω_4 as indicated by the MAC value of 0.990 in Fig. 17b. While there is relatively less, but still reasonably good correlation between the measured/predicted ODS at Ω_3 (MAC = 0.865). However, Fig. 17a shows that the relative vibration amplitude at blade 1 is not well captured by the GMM. Note that the GMM prediction to BTT measurement correlation result is in line with the modal verification result already illustrated in Fig. 10. Inadequate accuracy of the high mesh-density GMM in terms of the 1T blisk dynamics is the most likely reason for the minor discrepancy between the BTT measurements and GMM prediction. In addition, the remaining discrepancy could be also linked to the higher uncertainty of the BTT measurements due to the relatively lower vibration level of the 1T modes.

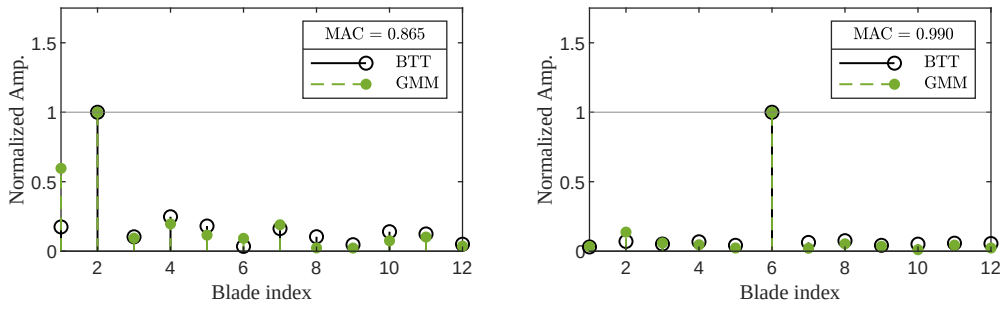

(a) ODS at Ω_3 (b) ODS at Ω_4

Figure 17: Comparison of tested/GMM predicted ODS at 1T mode/EO20 resonance in the spinning rig test.

5. Conclusions

This paper presents a full assessment of the dynamic prediction capability for the Geometrically Mistuned Models (GMMs) of an integrally manufactured blisk test piece. The GMMs are constructed upon the 3D optical geometry measurements and an FE mesh updating strategy. The high-fidelity, large-sized GMMs are proceeded into reduced-order models by the SMART approach for computationally efficient dynamic analyses.

The SMART approach is specifically tailored for the GMM fully mistuned by sector-level geometric variances with a relatively low memory requirement. In essence, it constructs the sector-level reduction mode basis by using only the truncated cyclic modes computed independently for each 'isolated' sector, with assumed cyclic symmetry at the sector interfaces. It combines the advantageous flexibility due to the 'substructuring' operation like the component-mode-based methods, and the cost-effective merit as the system-mode-based methods.

The GMMs in the form of SMART ROMs have been verfied and validated by intensive test campaigns in the well-controlled laboratory conditions. The high mesh-density GMM proves to be able to capture the modal dynamics and resonant vibration of the stationary/rotating blisk in terms of the 1B and 1T blisk modal family with a very good level of accuracy. It was also found that the accuracy of GMM exhibits a mode-related dependence on the mesh density. This is particularly true for the 1T mode family, which is featured by nearly blade-alone modes with low-level disk participation. The trade-off between model accuracy and prohibitive computational cost is the bottleneck of this promising geometric-mistuning modeling approach, which deserves evolutionary advancements in the future. In this regard, the application of the SMART approach as an efficient and accurate model reduction technique, has proven to be crucial.

The methods and correlation results presented in this paper are expected to push the frontier of the emerging geometric-mistuning modeling and dynamic analysis techniques based on the advanced 3D optical geometry measurement technology.

In essence, this research is also in line with the latest digital twin philosophy across the turbomachinery industry. Within this context, the physical-reality-based digital representation of the real aero-engine components through the precise geometry detection enables to evaluate their vibration behaviors in an effective way.

CRediT authorship contribution statement

Biao Zhou: Conceptualization, Methodology, Software, Investigation, Writing- Original draft, Funding acquisition, Project administration. **Chengyu Xie**: Software, Investigation. **Giuseppe Battiato**: Investigation, Writing- Reviewing and Editing. **Teresa Maria Berruti**: Supervision, Project administration, Writing- Reviewing and Editing.

Declaration of competing interest

The authors declare that they have no known competing financial interests or personal relationships that could have appeared to influence the work reported in this paper.

Acknowledgements

This work has received funding from the European Union's Horizon 2020 research and innovation program under the Marie Sklodowska-Curie grant agreement No. 891197. This work is also part of a project that has received funding from National Natural Science Foundation of China (Grant No. 52175098). This support is also gratefully acknowledged.

References

[1] E. Capiez-Lernout, C. Soize, J.-P. Lombard, C. Dupont, E. Seinturier, Blade manufacturing tolerances definition for a mistuned industrial bladed disk, Journal of engineering for gas turbines and power 127 (31) (2005). doi:10.1115/1.1850497.

[2] V. Ganine, M. Legrand, H. Michalska, C. Pierre, A sparse preconditioned iterative method for vibration analysis of geometrically mistuned bladed disks, Computers & Structures 87 (5) (2009) 342–354. doi:10.1016/j.compstruc.2008.12.011.

[3] R. Schnell, T. Lengyel-Kampmann, E. Nicke, On the impact of geometric variability on fan aerodynamic performance, unsteady blade row interaction, and its mechanical characteristics, Journal of Turbomachinery 136 (9) (2014) 091005–091005–14. doi:10.1115/1.4027218.

[4] V. Vishwakarma, A. Sinha, Forced response statistics of a bladed rotor with geometric mistuning, AIAA Journal 53 (9) (2015) 2776–2781. doi:10.2514/1.J053423.

[5] J. A. Beck, J. M. Brown, A. A. Kaszynski, E. B. Carper, Active subspace development of integrally bladed disk dynamic properties due to manufacturing variations, Journal of Engineering for Gas Turbines and Power 141 (2) (2018) 021001–021001–10. doi:10.1115/1.4040869.

[6] L. Carassale, A. Cavicchi, S. Bruzzone, M. Marrè Brunenghi, Probabilistic response of a bladed disk with uncertain geometry, Journal of Engineering for Gas Turbines and Power 141 (10) (2019). doi:10.1115/1.4044642.

[7] A. Sinha, B. Hall, B. Cassenti, G. Hilbert, Vibratory parameters of blades from coordinate measurement machine data, Journal of Turbomachinery 130 (1) (2008). doi:10.1115/1.2749293.

[8] V. Vishwakarma, A. Sinha, Y. Bhartiya, J. M. Brown, Modified modal domain analysis of a bladed rotor using coordinate measurement machine data on geometric mistuning, Journal of Engineering for Gas Turbines and Power 137 (4) (2015) 042502–042502–8. doi:10.1115/GT2018-76375.

[9] H. Schoenenborn, D. Grossmann, W. Satzger, H. Zisik, Determination of blade-alone frequencies of a blisk for mistuning analysis based on optical measurements, in: ASME Turbo Expo 2009: Power for Land, Sea, and Air, Vol. Volume 6: Structures and Dynamics, Orlando, Florida, USA, 2009. doi:10.1115/GT2009-59148.

[10] A. A. Kaszynski, J. A. Beck, J. M. Brown, Automated finite element model mesh updating scheme applicable to mistuning analysis, in: Turbomachinery Technical Conference and Exposition, Düsseldorf, Germany, 2014, p. V07BT33A025. doi:10.1115/GT2014-26925.

[11] T. Backhaus, T. Maywald, S. Schrape, M. Voigt, R. Mailach, A parametrization describing blisk airfoil variations referring to modal analysis, in: Turbomachinery Technical Conference and Exposition, Vol. Structures and Dynamics, Charlotte, NC, USA, 2017, p. V07AT32A003. doi:10.1115/GT2017-64243.

[12] C. Meckstroth, J. Brown, Point cloud to parameter: An inverse geometric approach to probabilistic design, in: ASME Turbo Expo 2019: Turbomachinery Technical Conference and Exposition, Vol. Volume 7A: Structures and Dynamics, Phoenix, Arizona, USA, 2019, p. V07AT32A007. doi:10.1115/GT2019-91652.

[13] T. Maywald, T. Backhaus, S. Schrape, A. Kühhorn, Geometric model update of blisks and its experimental validation for a wide frequency

range, in: ASME Turbo Expo 2017: Turbomachinery Technical Conference and Exposition, Charlotte, North Carolina, USA, 2017, p. V07AT30A001. doi:10.1115/GT2017-63446.

[14] A. A. Kaszynski, J. A. Beck, J. M. Brown, Automated meshing algorithm for generating as-manufactured finite element models directly from as-measured fan blades and integrally bladed disks, in: Turbomachinery Technical Conference and Exposition GT2018, Vol. Structures and Dynamics, Oslo, Norway, 2018, p. V07CT35A024. doi:10.1115/GT2018-76375.

[15] J. Yuan, F. Scarpa, G. Allegri, B. Titurus, S. Patsias, R. Rajasekaran, Efficient computational techniques for mistuning analysis of bladed discs: A review, Mechanical Systems and Signal Processing 87 (2017) 71–90. doi:10.1016/j.ymssp.2016.09.041.

[16] A. Tacher, F. Thouverez, J. Armand, Modelling and analysis of a bladed drum subject to the coriolis and mistuning effects, International Journal of Mechanical Sciences 215 (2022) 106994. doi:10.1016/j.ijmecsci.2021.106994.

[17] E. B. Henry, J. M. Brown, J. C. Slater, A fleet risk prediction methodology for mistuned ibrs using geometric mistuning models, in: 17th AIAA Non-Deterministic Approaches Conference, Vol. Random Fatigue, Fracture and Life Prediction, American Institute of Aeronautics and Astronautics, 2015, p. 1144. doi:10.2514/6.2015-1144.

[18] H. Bae, I. M. Boyd, E. B. Carper, J. Brown, Accelerated multifidelity emulator modeling for probabilistic rotor response study, Journal of Engineering for Gas Turbines and Power 141 (12) (2019). doi:10.1115/1.4045019.

[19] A. A. Kaszynski, J. M. Brown, Accurate blade tip timing limits through geometry mistuning modeling, in: Turbine Technical Conference and Exposition, Montréal, Canada, 2015, p. V07AT27A007. doi:10.1115/GT2015-43192.

[20] J. A. Beck, A. A. Kaszynski, J. M. Brown, D. L. Gillaugh, O. E. Scott-Emuakpor, Selection of dynamic testing measurement locations for integrally bladed disks, in: Turbomachinery Technical Conference and Ex-

position GT2018, Vol. Structures and Dynamics, Oslo, Norway, 2018, p. V07CT35A037.

[21] D. L. Gillaugh, A. A. Kaszynksi, T. C. Tomlin, J. M. Brown, J. A. Beck, E. B. Carper, Accurate blade tip timing placement on a centrifugal impeller using as-manufactured modeling, in: ASME Turbo Expo 2022: Turbomachinery Technical Conference and Exposition, Vol. Volume 8B, American Society of Mechanical Engineers, 2022, p. V08BT27A035.

[22] M. Gambitta, A. Kühhorn, S. Schrape, Geometrical variability modelling of axial compressor blisk aerofoils and evaluation of impact on the forced response problem, in: Turbo Expo: Power for Land, Sea, and Air, Vol. 84096, American Society of Mechanical Engineers, 2020, p. V02DT38A028. doi:10.1115/GT2020-16168.

[23] M. Gambitta, B. Beirow, S. Schrape, A digital twin of compressor blisk manufacturing geometrical variability for the aeroelastic uncertainty quantification of the aerodynamic damping, in: Turbo Expo: Power for Land, Sea, and Air, Vol. 86069, American Society of Mechanical Engineers, 2022, p. V08AT21A021. doi:10.1115/GT2020-16168.

[24] J. A. Beck, J. M. Brown, C. J. Cross, J. C. Slater, Component-mode reduced-order models for geometric mistuning of integrally bladed rotors, AIAA Journal 52 (7) (2014) 1345–1356.

[25] J. A. Beck, J. M. Brown, A. A. Kaszynski, C. J. Cross, J. C. Slater, Geometric mistuning reduced-order models for integrally bladed rotors with mistuned disk-blade boundaries, Journal of Turbomachinery 137 (7) (2015) 071001. doi:10.1115/1.4029122.

[26] J. A. Beck, J. M. Brown, A. A. Kaszynski, D. L. Gillaugh, Numerical methods for calculating component modes for geometric mistuning reduced-order models, Journal of Engineering for Gas Turbines and Power 144 (3) (2021). doi:10.1115/GT2021-59126.

[27] A. Sinha, Reduced-order model of a bladed rotor with geometric mistuning, Journal of Turbomachinery 131 (3) (2009) 031007. doi:10.1115/1.2987237.

[28] M. Mbaye, C. Soize, J.-P. Ousty, A reduced-order model of detuned cyclic dynamical systems with geometric modifications using a basis of

cyclic modes, Journal of engineering for gas turbines and power 132 (11) (2010).

[29] S. Baek, B. Epureanu, Reduced-order models of blisks with small geometric mistuning, Journal of Vibration and Acoustics 139 (4) (2017) 041003–041003–10. doi:10.1115/1.4036105.

[30] L. Carassale, M. Maurici, Interface reduction in craig–bampton component mode synthesis by orthogonal polynomial series, Journal of Engineering for Gas Turbines and Power 140 (5) (2017).

[31] J. de Cazenove, S. Cogan, M. Mbaye, Finite-element modelling of an experimental mistuned bladed disk and experimental validation, in: Turbomachinery Technical Conference and Exposition GT2013, Vol. Volume 7B: Structures and Dynamics, San Antonio, Texas, USA, 2013, p. V07BT31A016. doi:10.1115/GT2013-95985.

[32] A. Kaszynski, J. Brown, J. Beck, Experimental validation of an optically measured geometric mistuning model using a system id approach, in: 17th AIAA Non-Deterministic Approaches Conference, Kissimmee, Florida, US, 2015, p. V07CT35A024.

[33] T. Maywald, C. Heinrich, A. Kühhorn, S. Schrape, T. Backhaus, Prediction of geometrically induced localization effects using a subset of nominal system modes, in: ASME Turbo Expo 2019: Turbomachinery Technical Conference and Exposition, Vol. Volume 7B: Structures and Dynamics, Phoenix, Arizona, USA, 2019, p. V07BT35A012. doi:10.1115/GT2019-90884.

[34] D. L. Gillaugh, A. A. Kaszynski, J. M. Brown, J. A. Beck, J. C. Slater, Mistuning evaluation comparison via as-manufactured models, traveling wave excitation, and compressor rigs, Journal of Engineering for Gas Turbines and Power 141 (6) (2019).

[35] D. L. Gillaugh, T. J. Janczewski, A. A. Kaszynski, J. M. Brown, J. A. Beck, C. Nessler, Forced response variation of a compressor utilizing blade tip timing, strain gages, and as-manufactured finite element models, Journal of Engineering for Gas Turbines and Power 143 (11) (2021).

[36] B. Zhou, T. M. Berruti, A novel model reduction approach for blisks with blend repairs and small mistuning, Mechanical Systems and Signal Processing 195 (2023) 110308. doi:10.1016/j.ymssp.2023.110308.

[37] B. Zhou, J. Zhao, T. M. Berruti, Exploration of blade detuning tests for mistuning identification of blisks, Mechanical Systems and Signal Processing 175 (2022) 109118.

[38] A. A. Kaszynski, J. A. Beck, J. M. Brown, Uncertainties of an automated optical 3d geometry measurement, modeling, and analysis process for mistuned integrally bladed rotor reverse engineering, Journal of Engineering for Gas Turbines and Power 135 (10) (2013) 102504. doi:10.1115/1.4025000.

[39] B. Zhou, J. Zhao, N. Ye, T. M. Berruti, Blisk with small geometry mistuning and blend repair: As-measured finite element model and experimental verification, Journal of Engineering for Gas Turbines and Power 144 (10) (2022) 101017.

[40] A. A. Kaszynski, J. A. Beck, J. M. Brown, Experimental validation of a mesh quality optimized morphed geometric mistuning model, in: ASME Turbo Expo 2015: Turbomachinery Technical Conference and Exposition, Montréal, Canada, 2015, p. V07AT27A005.

[41] Y. J. Chan, D. J. Ewins, Prediction of vibration response levels of mistuned integral bladed disks (blisks): Robustness studies, Journal of Turbomachinery 134 (4) (2011). doi:10.1115/1.4003646.

[42] T. Berruti, C. M. Firrone, M. M. Gola, A test rig for noncontact traveling wave excitation of a bladed disk with underplatform dampers, Journal of Engineering for Gas Turbines and Power 133 (3) (2010).

[43] C. M. Firrone, T. Berruti, An electromagnetic system for the noncontact excitation of bladed disks, Experimental Mechanics 52 (5) (2012) 447–459.

[44] G. Battiato, C. M. Firrone, T. M. Berruti, Forced response of rotating bladed disks: Blade tip-timing measurements, Mechanical Systems and Signal Processing 85 (2017) 912–926. doi:10.1016/j.ymssp.2016.09.019.

Declaration of interests

☒The authors declare that they have no known competing financial interests or personal relationships that could have appeared to influence the work reported in this paper.

☐The authors declare the following financial interests/personal relationships which may be considered as potential competing interests: